Optical and Photocatalytic Properties of Fe^{3+}-Doped Tio_2 Thin Films Prepared by a Sol–Gel Dip-Coating

Mohamed Cherif Benachour[1,3]*, Hichem Sedratia[2], Rahima Zellaghi[1], Fayssal Boufelgha[1], Heider Dehdouh[1], Hakim Fatmi[1], and Rabeh Bensaha[3]

[1]Research Center in Industrial Technologies CRTI, P. O. Box 64, Cheraga, Algiers, 16014 Algeria.

[2]Laboratoire d'Anticorrosion, Matériaux Et Structure (LAMES), Faculté des Sciences, Université 20 Août 1955, BP 26 Route El-Hadaïk, Skikda 21000, Algeria.

[3]Ceramics laboratory, Frères mentouri-Constantine-1 University, Road Ain El-Bey, 25000 Constantine, Algeria.

*E-mail: benachour25cherif@gmail.com

Received: 12 May 2023; Accepted: 27 August 2023; Published: 10 September 2023

Abstract:

The present work focuses on the effect of doping on the synthesis, characterization and photocatalytic activity of TiO_2 thin films doped with iron at different percentages by the sol–gel method and characterized by using techniques such as x-ray diffraction (XRD), scanning electron microscopy (SEM), UV–visible spectroscopy and Fourier transform infrared (FTIR). and photocatalytic degradation of Rhodamine B under the sunlight. The XRD results revealed that the synthesized samples are pure and crystalline in nature and show a tetragonal anatase phase of TiO_2, Moreover, also revealed that the crystallinity and crystal size increasing with increasing Fe^{3+} percentage due to the aggravation of anatase TiO_2 crystallinity. SEM microscopic images showed that all the well-adhesive Fe^{3+} Doped TiO_2 thin films had homogeneous and smooth surfaces, contained granular nanocrystals, and without cracks. The UV–vis absorption spectra showed that the absorption of the TiO_2 thin films had a small red-shift as the Fe^{3+} percentage increased. The direct band gap energy (Eg) of Fe^{3+}-doped TiO_2 thin films decreased with increasing Fe^{3+}-doping . this behavior is attributed to the Fe^{3+}, whose presence decrease the band gap and could stabilize the separation between the photogenerated electron-hole pair. Moreover, the rate constant of Rhodamine B decomposition increased as the Fe^{3+} percentage increased. Fe^{3+} doped TiO_2 exhibited enhanced photocatalytic efficiency compared to pristine TiO_2, attributed to improved charge separation and higher electron-hole pair generation.

Keywords: Fe^{3+}-doped TiO_2, sol-gel dip coating, Thin-films, photocatalytic activity.

Tob Regul Sci. ™ 2023 ;9(1): 5413 - 5430

DOI: doi.org/10.18001/TRS.9.1.378

I. Introduction:

Furthermore, Schrauzer and Guth [46] were among the first to describe the synthesis of Fe-doped TiO_2 and Fe-free powders via an impregnation process, followed by calcination at 1273 K. The incorporation of Fe ions resulted in a noticeable enhancement of the TiO_2 powders' photocatalytic activity [39, 40].

imperative to eradicate pollutants underscores the pressing need to explore novel catalyst materials with enhanced properties and efficiency [1]. In the face of the conventional treatment's ineffectiveness against these recalcitrant contaminants, recent efforts have turned towards Advanced Oxidation Processes (AOPs) as promising alternatives. Among these, photocatalysis stands out as a contemporary technique for remediating water resources.

Photocatalysis entails the generation of highly oxidative radical species within the medium. To initiate this process, a solid semiconductor must be activated by sufficiently energetic radiation. In this context, the solid material assumes the role of a photocatalyst, facilitating the generation of hole-electron pairs under irradiation. These electron-hole pairs are instrumental in the formation of radical species that, in turn, drive the degradation and mineralization of contaminants [2, 3].

In recent years, the photocatalytic degradation of aqueous organic pollutants and gaseous formaldehyde by Titanium Dioxide (TiO_2) has garnered substantial attention in the realm of environmental protection. This heightened interest can be attributed to TiO_2's advantageous optical and electronic properties, chemical stability, non-toxicity, and cost-effectiveness [4].

However, TiO_2 exhibits a considerable energy band gap of 3.2 eV, which restricts its activation solely to the ultraviolet (UV) range. Consequently, its efficacy as a photocatalyst using visible light is markedly limited, with a mere 5% of sunlight utilization [5, 6].

To address this limitation, various strategies have been explored, including the incorporation of noble metals such as gold [7] and silver [8-11], transition metals like Fe [12-15], Cr [16], Cu [17], Mn [18], Zn [19, 20], and V [21-24], as well as non-metals like nitrogen [28-31] and carbon [31]. Notably, TiO_2 particles can be doped with Iron (Fe) to create a composite material at low Iron concentrations. Given the similar ionic radii of Fe^{3+} and Ti^{4+} ions (0.64 Å and 0.68 Å, respectively), the substitution of Iron cations for titanium within the TiO_2 lattice is a facile process.

Nevertheless, the widespread application of photocatalysis for industrial wastewater treatment is hindered by its relatively low reaction rate, primarily attributable to the rapid recombination of

charge carriers [4]. This limitation stems from TiO_2 high energy band gap, which confines its light absorption mainly to the UV spectrum, with wavelengths shorter than 387.5 nm. Consequently, the high rate of electron-hole pair recombination results in low quantum efficiency and a constrained photooxidation rate [32-34]. The photocatalytic attributes of TiO_2 are profoundly influenced by sample preparation conditions, crystal phase, surface area, size distribution, porosity [35,36], and the presence of additional components such as metal particles, which are employed to enhance catalytic response [35]. Notably, anatase TiO_2 demonstrates superior photocatalytic activity compared to rutile TiO_2.

Over the past two decades, extensive research has been dedicated to extending TiO_2 light absorption into the visible region and mitigating the recombination of excited electron-hole pairs. This has led to the exploration of various approaches, including doping with different elements [32, 35, 37–41], surface modifications [42-44], and diverse preparation methods [37–40, 42, 45], as reported by numerous researchers. Furthermore, Schrauzer and Guth [46] were among the first to describe the synthesis of Fe-doped TiO_2 and Fe-free powders via an impregnation process, followed by calcination at 1273 K. The incorporation of Fe ions resulted in a noticeable enhancement of the TiO_2 powders' photocatalytic activity [39,40].

Conversely, nanocrystalline TiO_2 thin films are typically synthesized from alkoxide solutions through methods like physical vapor deposition (PVD) [47], chemical vapor deposition (CVD) [48], and dip coating [49]. Surprisingly, despite the extensive body of literature, a comprehensive elucidation of the impact of Fe^{3+} doping on the optical and photocatalytic properties of TiO_2 thin films prepared through sol–gel dip coating remains conspicuously absent [37].

In the present investigation, we delve into the influence of Fe^{3+} doping on the optical, photocatalytic, and microstructural attributes of sol–gel dip-coated TiO_2 thin films. The photocatalytic efficacy was evaluated by monitoring the degradation of Rhodamine B dye under sunlight, revealing a remarkable enhancement with increasing Fe3+ content. This phenomenon underscores the superior photocatalytic efficiency of Fe^{3+}-doped TiO_2 thin films compared to pristine TiO_2. Our study aims to fill the existing gap in the optimization of these materials using the sol-gel method, driven by the promising potential offered by the introduction of Fe^{3+}. Additionally, we employ X-ray Diffraction (XRD), Scanning Electron Microscopy (SEM), UV–Visible Spectroscopy, and Fourier Transform Infrared (FTIR) analysis to discern the distinctive characteristics of these materials.

II. Experimental procedure:

The sol-gel process, at its core, relies on the transformation of a liquid-phase solution containing precursors into a solid material through a series of chemical polymerization reactions conducted at ambient temperature [50]. To achieve a solution conducive for dipping, the sol preparation

entails a sequential approach. In the initial step, a transparent solution is formulated by dissolving one mole (1 mol) of butanol (C_4H_9OH) as a solvent, coupled with the addition of four moles (4 moles) of acetic acid ($C_2H_4O_2$). Furthermore, one mole (1 mol) of distilled water is introduced, along with one mole (1 mol) of tetrabutyl–orthotitanate $(C_4H_9O)_4Ti$ [51, 52]. This meticulously concocted solution, characterized by its transparency tinged with a gentle yellow hue, serves as the foundational precursor for subsequent stages.

In the second phase, the process commences with the dissolution of high-purity iron powder (99%) in a 1% hydrochloric acid solution, yielding a solution of iron chloride ($FeCl_3$). Following this, in the third phase, the solutions of titanium dioxide (TiO_2) are doped with varying concentrations of $FeCl_3$, specifically 0.5% and 1%.

The deposition method employed throughout this study is the dip-coating technique. To ensure the substrates possess a refractive index of 1.52, meticulous cleaning procedures were executed. Subsequently, these prepared substrates were immersed successively in the solutions of undoped and Fe^{3+}-doped TiO_2, each for a duration of 10 minutes. The withdrawal process was meticulously controlled at a speed of 0.625 $cm.s^{-1}$ [51, 53, 54]. Post-dipping, the films underwent a drying phase at 100 °C for 10 minutes after each deposition. Finally, the treated samples were subjected to a temperature at 500 °C, maintaining this condition for a duration of one hour.

Characterization of the thin films was executed through various techniques. The structural evolution of the films was meticulously monitored employing a Brunkers Axs Advanced diffractometer, utilizing Cu (Kα) radiation with a wavelength (λ) of 1.54056 Å. The angular range spanned from 10° to 70°, with an incidence angle of 2θ = 0.5°.

The surface morphology and thickness of TiO_2 thin films doped and not doped with Fe^{3+} were concluded by scanning electron microscopy (SEM).

UV absorption studies were conducted using a UV–vis double-beam spectrophotometer, specifically the SHIMADZU (UV3101PC), capable of spanning wavelengths from 190 to 3200 nm. Data analysis and spectral treatment were performed utilizing the UVPC software.

The set up used for photocatalytic reaction tests has been described.

III. Results and discussion:

III. 1. X-ray diffraction (XRD):

In order to ensure the structural quality of the samples, we performed measurements from X-ray diffraction. The films were analyzed by X-ray diffraction (XRD). We have followed the structural evolution of TiO_2 thin films as a function of undoped titanium oxide as well as four different

concentrations of iron chloride (0%, 0.5% and 1%). X-ray diffraction allowed us to determine crystal quality, evaluate constraints, measure grain size,...etc.

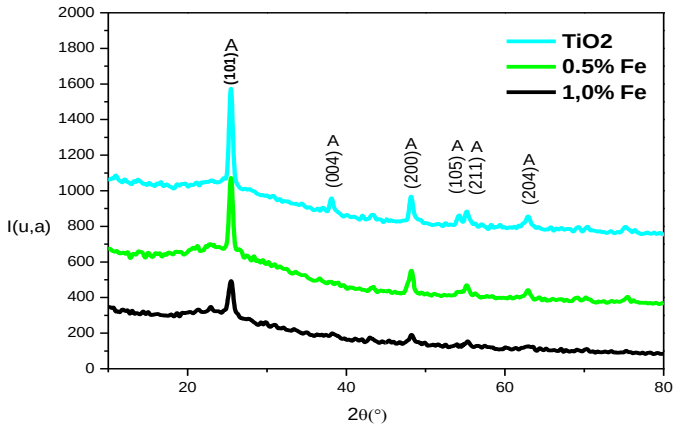

Figure.1. X-ray diffraction spectra of TiO_2 thin films doped and not doped with Fe^{3+} in different proportions (0%, 0.5%, 1%) annealed at 500°C for 1h.

Fig.1 shows the results of the X-ray diffraction pattern of samples deposited with a TiO_2 layer and annealed at 500°C for 1h shows the beginning of crystallization of the titanium oxide compound with the appearance of the anatase phase, and this is consistent with the results of other work.

These results confirmed that TiO_2 doped with Fe^{3+} displays a tetragonal crystal structure with an anatase phase (one, the resolved diffraction peaks were characterized using Miller indices, we obtained 25.4, 48.05, 37.9, 54.355.3, 62.85 which correspond to levels (101). (004), (200), (105), (211), (204), respectively, as we find that the (101) level is the preferred crystal growth direction.

We also notice that there are no peaks of iron or iron oxide, and this is due to the small percentage of iron concentration, and the X-ray diffraction device cannot detect small percentages of doping. We also note that the iron doping process led to an increase in the width of the titanium oxide peaks.

The average size of the crystals was calculated using Scherrer's [55,56] formula, the results demonstrate a notable trend: as the graft concentration increases, there is a corresponding rise in the average crystal size, transitioning from 12,768 nanometers to 15,728 nanometers. Additionally, a distinct reduction in the peak at (2Θ = 25.4) is observed.

Furthermore, the intensity and breadth of the peak width provide valuable insights. These characteristics suggest that the enlargement of the crystals might be attributed to the integration of iron ions into the cation sites within the TiO_2 structure.

It was calculated using the relationship:

$d_{hkl} = n\lambda / 2\sin\theta$

λ: X-ray wavelength.

n: diffraction rank.

d_{hkl} : The distance between the crystal planes.

Θ: Bragg angle diffraction of X-ray samples.

The following table shows the grain size of doped and undoped TiO_2:

Percentage of TiO_2 doping $FeCl_3$	2Θ(°)	the level (hkl)	grain size d(nm)
00%	25.452	25.452	12,768
0.5%	25.478	25.478	14,034
1%	25.467	25.467	14,861

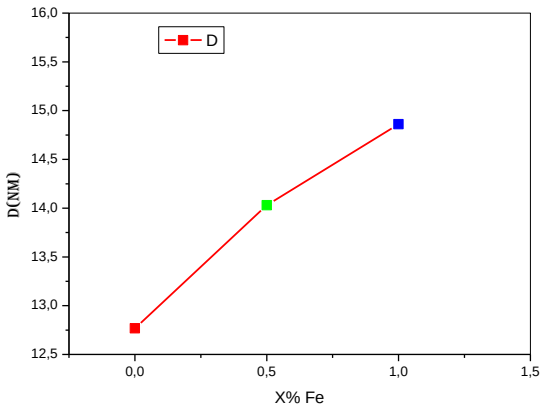

Figure.2. The grain size change of TiO_2 doped and undoped with Fe^{3+} in different percentages (0%, 0.5%, 1%) annealed at 500°C for 1h.

The ionic radius of iron is (0.064 nm), which is very close to the ionic radius of Ti^{4+} (0.068 nm), which also means that Fe^{3+} can enter the structure of TiO_2 and replace Ti^{4+}. The DRX results can be explained by the fact that there is no difference in the retina between the iron-unsaturated TiO_2 nanoparticles.

III. 2. FTIR Spectrum Analysis:

The study was carried out using Fourier transform infrared absorption spectroscopy to understand the behavior of the material resulting from heat treatments. Some experiments

showed that layers with a thin thickness have good permeability to infrared rays, unlike thick layers, as the frequency range (2500-520) was scanned inside a device from Type (JASCO (FT/IR-6300) so that any absorbed frequency characterizes the type of vibration of a particular bond. We will use this property to track the distinct bonds of the Ti-O and Ti-O-Ti samples in the thin layers of TiO_2. For this we will look at the low frequencies that are in the range (400-800 cm^{-1}) It is the field of presence of these bonds and the extension of the chain [Ti-O-Ti-O-Ti-O], which is the field specified by Devitt (Me) [57].

Larbot, Chhor, and others [58,59] have divided this frequency into two areas:

• A range [550-653 cm^{-1}] in which the Ti-O bond frequencies extend.

• A range [436-495 cm^{-1}] in which the frequencies of the Ti-O bond and the Ti-O-Ti bond within the polymer chain extend [Ti-O-Ti-O-Ti-O].

The Ti-O-Ti and O-Ti-O structural bonds are the characteristic bonds of titanium dioxide crystallization, while the high-frequency field corresponds to the vibration of the bonds of water and organic molecules.

Fig.3 shows the infrared spectra of Fe^{3+}-doped TiO_2 thin films deposited on glass substrates obtained for annealing temperature for 1 hours.

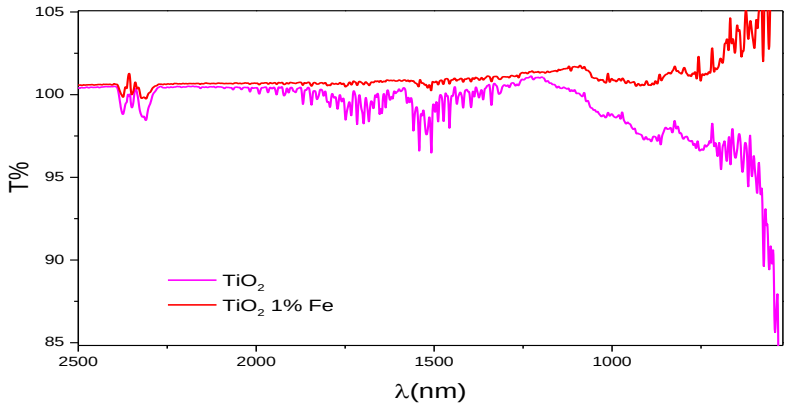

Figure.3. Infrared spectra of TiO_2 thin films doped with Fe^{3+} in different proportions (0%, 1%) annealed at 500°C for 1h.

We also relied in our study on the results of previous studies that the vibration bond between iron and oxygen belongs to the range [400-750 cm^{-1}] [60], and due to the small rates of vaccination, this association was not found with us.

Where we notice the presence of two values at 573.68 and 829.76 cm^{-1}, which correspond to Ti-O and Ti-O-Ti, respectively, and which belong to the anatase phase, then the infrared analysis

confirms the information we obtained from the X-ray analysis, which shows the presence of anatase type titanium oxide.

III .3 .Analysis of the results of scanning electron microscopy (MEB):

To study the surface morphology of our sediments with the variation of ferric chloride concentration, a scanning electron microscope was used to get an idea of the surface condition of the prepared samples that we chose at a concentration of (0%, 0.5%, 1%) for different purposes. SEM images of doped and undoped TiO_2 films:

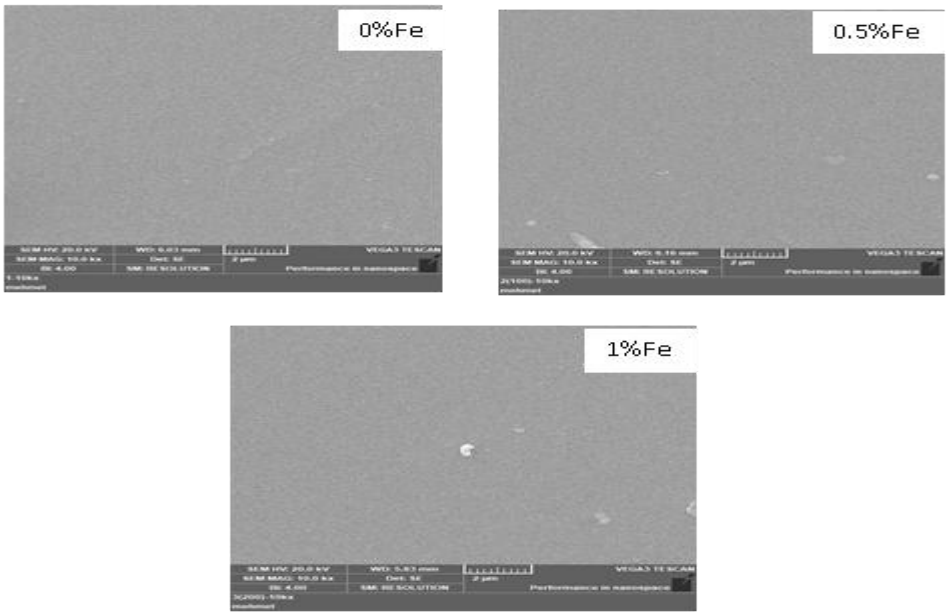

Figure.4. SEM micrographs of TiO_2 thin films doped and undoped with Fe^{3+} in different percentages (0%, 0.5%, 1%) annealed at 500°C for 1h.

Microscopic images (Fig.4) show that the thin layer of TiO_2 is inlaid with different percentages of Fe^{3+} (0%, 0.5%, 1%) that is homogeneous and has a surface state without cracking on the entire surface of the sample when annealing at a temperature 500°C. The observations reflect the fact that the stresses introduced by temperature during crystallization are not so great as to degrade the surface continuity of the thin film. One of the aspects related to the surface morphology is the porosity, where the SEM images of the Fe^{3+}- doped TiO_2 thin film shows different growth of the pore structures in the film as we also note that the amount of pores is large and of different shapes.

III.4 .Characterizations by transmission UV-Vis spectrometer:

III .4. 1 Analysis of transmittance spectra:

We know that titanium oxide represents the visible light spectrum with a high diffusion coefficient without an absorption region, with 96% of the light energy from which the incident

will be reflected. TiO_2 has been shown to be insensitive to visible light, due to its broad forbidden band, which allows it to absorb near ultraviolet.

The optical properties included a study of the effect of Fe^{3+} concentration, in molar percentages (0%, 0.5%, 1%) on the optical properties of the TiO_2 layers. The transmittance spectrum of the layers was measured within wavelengths (300-1000nm). Transmittance T as the ratio of the transmitted intensity to the incident intensity. In addition, using this type of spectrum allows us to arrive at the determination of the film thickness, as well as some other optical properties: the optical absorption threshold, the optical gap, the refractive index, and the porosity of the material. The results showed that there is a clear increase in the transmittance values as a function of wavelength. As these results showed that the layers of titanium oxide have a permeability rate of approximately 90%, as the value of transparency increases and reaches within the near visible spectrum region, with a little permeability in the ultraviolet region, which increases sharply at the value (380-400), and this region is called At the main absorption edge with a slight deviation in the case of absorption towards higher energies, and this in turn indicates that the material is a semi-conductor with a wide energy gap.

In Fig.5 we can say that increasing the grafting rates led to an increase in the granular growth process, that is, an increase in the size of the granules, which led to a decrease in light scattering.

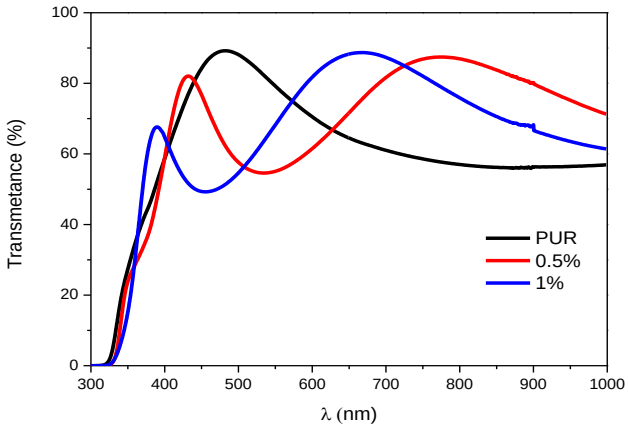

Figure. 5. The transmittance spectrum of TiO_2 thin films doped and undoped with Fe^{3+} in different percentages (0%, 0.5%, 1%) annealed at 500°C for 1h.

It was shown from the permeability curves that with increasing grafting rates, we notice that there is a decrease in the permeability values, and this indicates that grafting with iron atoms has led to an increase in the donor levels near the transport band. And (Fig.5) shows a decrease in the permeability values, and this is due to the thickness of the sample, as it is proportional to the Pere Lombert law, that the permeability is inversely proportional to the thickness, as shown in the relationship:

$T=(1-R)\ e^{-\alpha d}$

III.4.2. Determine the energy gap:

In the UV field, a sudden decrease in the transmittance of films is due to the fundamental absorption of light, corresponding to transitions between bands, for example the excitation of an electron from the valence band to the conduction band beyond the fundamental absorption threshold. The determination of the energy gap is based on the model associated with the absorption coefficient α :

$$(\alpha h\upsilon)^2 = A(h\upsilon - E_g)$$

Where hυ is the photon energy, α is the absorption coefficient, Eg the band gap energy and A is a constant.

The band gap values for Fe^{3+}- doped TiO_2 thin films are shown in Fig.6.

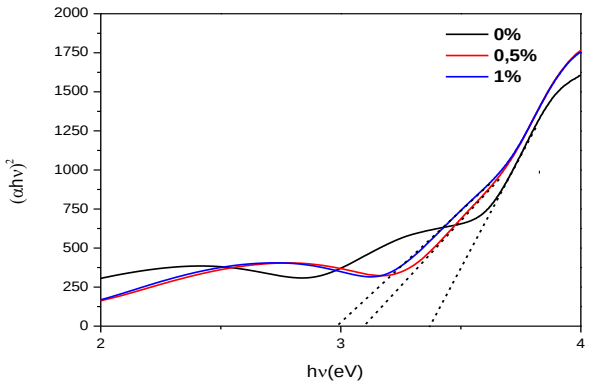

Figure.6. Determination of the energy gap by extrapolation from the anisotropy of $(\alpha h\nu)^2$ as a function of hν.

By drawing the relationship from $(h\nu\alpha)^2$ and the incident photon energy hν, the linear part is simulated by drawing the tangent that intersects the axis of the separators at the value of the energy gap. The following table shows the energy gap values for TiO_2 thin films doped with Fe^{3+} (0 %, 0.5%, 1%,)

Doping rate	Energy gap (eV)
0%	3.37
0.5 %	3.10
1%	2.97

We notice from the energy gap values that the higher the doping percentage, the smaller the energy gap, which indicates that iron is a good agent for reducing the energy gap value of titanium dioxide.

III.5. Analysis of the photocatalytic test:

In this test, we prepared a solution of rhodamine with RhB, and then stirred the solution under sunlight for 30 minutes. RhB was used as a light indicator. The photocatalytic activity of TiO_2 and TiO_2 doped with Fe^{3+} (0.5% 1%) was examined.

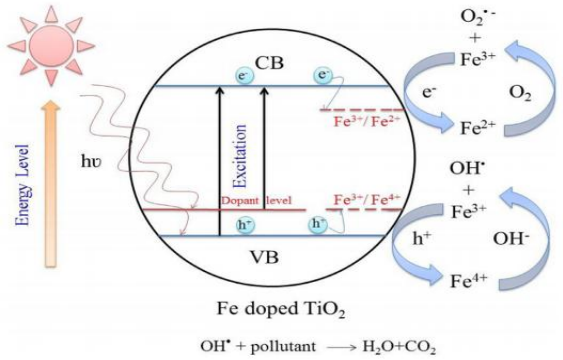

Figure.7. shows the schematic diagram of the photocatalytic process on Fe^{3+}-doped TiO_2 thin films

Fig.8, which represents the absorption spectrum of Rhodamine B with the chemical formula $C_{28}H_{31}C_lN_2O_3$. We distinguish the presence of a major peak at the wavelength of 554 nm in the spectral range (400-800 nm).

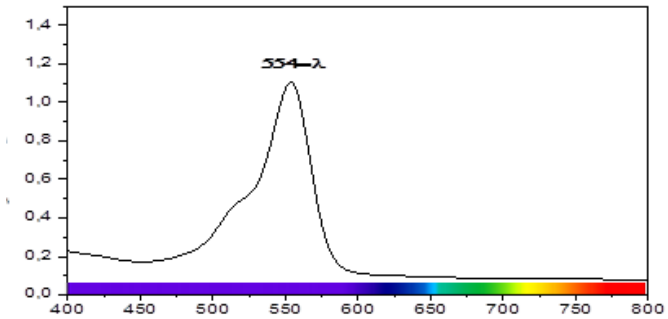

Figure.8. Color absorption spectrum of Rhodamine B (RhB)

The catalytic behavior of samples prepared from titanium oxide doped with iron(III) titanium oxide, obtained by a Sol-gel method, was studied. We used a concentration of 10^{-4} of the rhodamine B dye, placed the samples in a certain volume of water contaminated with the dye, exposed them to sunlight with continuous magnetic stirring, and then We analyzed the absorbance every 30 minutes over a period of 3 hours and obtained the curves (Fig.9.a).

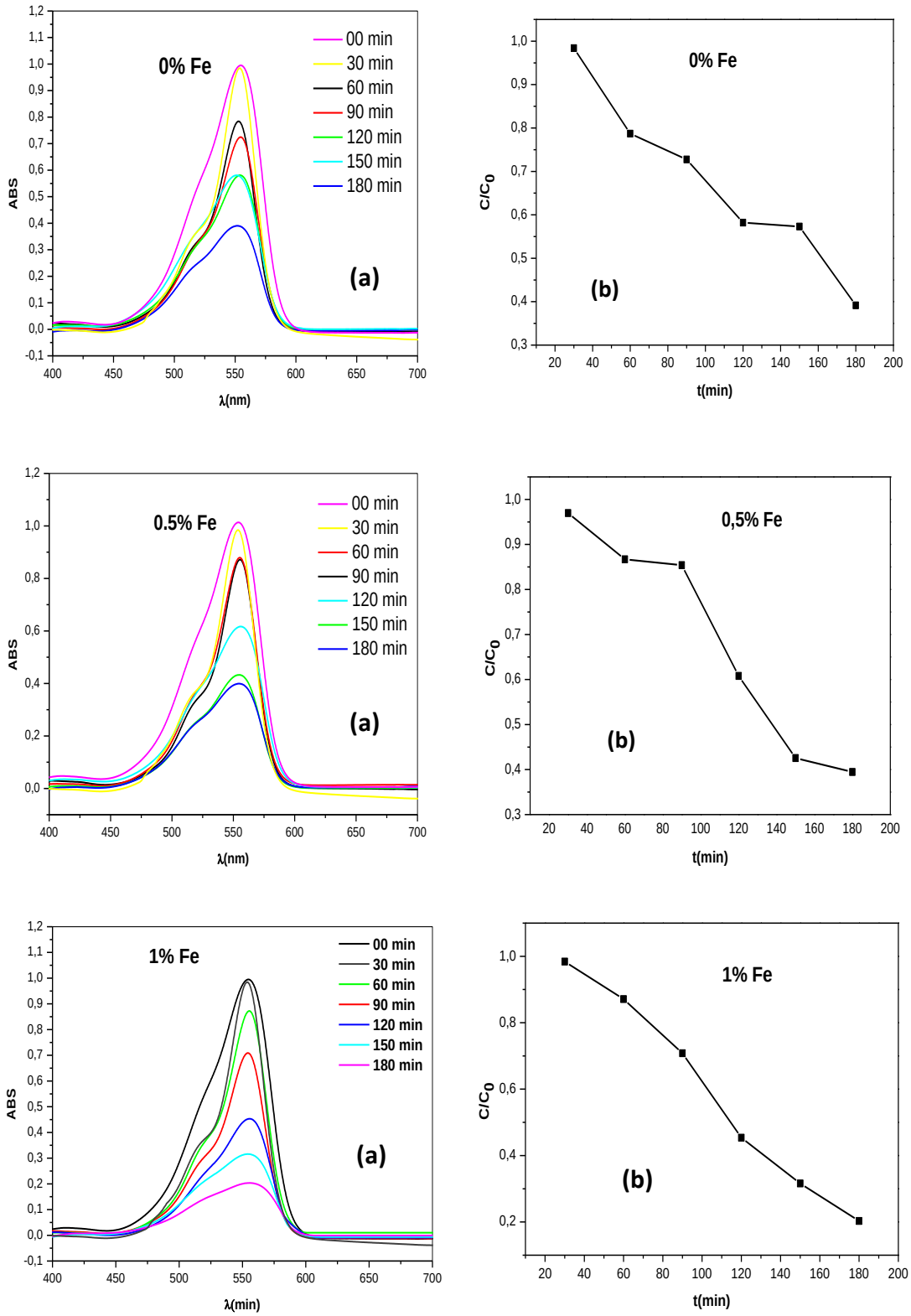

Figure 9.a. Representative absorption curves for the degradation of rhodamine B after times under sunlight, in the presence of Fe^{3+}-doped and undoped TiO_2 particles obtained by sol-gel, Figure 9. b represents the change in the concentration of radiamine B solution with the change of time for both doping and non doping samples.

The catalytic behavior of the samples prepared from iron-doped titanium oxide obtained by sol-gel method was studied. We used a concentration of 10^{-4} of the rhodamine B dye and placed the samples in a certain volume of water contaminated with the dye and exposed them to sunlight with continuous magnetic stirring. Then we analyzed the absorbance every 30 minutes over a period of 3 hours, and we obtained the curves (Fig.9.a). We measured the concentration ratio (C/C_0) as a function of time, after establishing the adsorption-desorption equilibrium for 30 minutes (Fig.9.b).

The function $f(t) = C/C_0$ was shown at different time intervals during the degradation process of Rhodamine B, where the highest rate of degradation occurred during the first 30 minutes of photocatalysis after which it decreased in a linear manner. This means that the analyzed system modifies the mechanism by which it occurs. The color degradation process studied, which indicates the effectiveness of the photocatalyst to remove this pollutant from water.

The percentage of photocatalytic efficiency of rhodamine B aqueous solution in inlaid and ungrafted TiO_2 samples can be calculated using the equation [61]:

$$ή = \frac{C - C0}{C0}.100\%$$

Where it represents:

ή: :Organic decomposition rate (expressed as a percentage).

C_0: Concentration of the initial coloring solution.

C : The concentration of the coloring solution after a certain period of photodegradation.

The photocatalytic result 1 hour after the dispersion of the undoped and doped TiO_2 system under sunlight indicates that the incorporation of iron into the TiO_2 matrix has a positive effect on the photocatalytic activity of TiO_2 for the anatase phase.

Conclusion:

In conclusion, this study provides a comprehensive exploration of the characteristics and optical properties of iron ion (Fe^{3+}) doped titanium oxide thin films produced through the sol-gel spin coating technique. Our findings underscore the potential of these films for a wide range of applications, including photocatalysis, sensors, and photovoltaics. Moreover, the study sheds light on the intricate interplay between dopant concentration, processing parameters, and material properties, offering valuable insights for future research and development in this field.

References:

[1] Justicia, G. Garcia, G.A. Battiston, R. Gerbasi ,F. Ager, M. Guerra, J. Caixach, J.A .Pardo, J. Rivera, A. Figueras, Photocataly sis in the visible range of sub-stoichiometric anatase films prepared by MOCVD, Electrochim. Acta 50 (2005) 4605–4608.

[2] Saud P S, Pant B, Alam Al-M, Ghouri Z K, Park M and Kim H-Y 2015 Ceram. Int. 41 11953–9

[3] Sun T, Fan J, Liu E, Liu L, Wang Y, Dai H, Yang Y O, Hou W, Hu X and Jiang Z 2012 Powder Technol. 228 210–21

[4] T. Noguchi, A. Fujishima, P. Sawunyama, K. Hashimoto, Photocatalytic degradation of gaseous formaldehyde using TiO2 film, Environ. Sci. Technol. 32 (1998) 3831–3833.

[5] Cermenatti, L.; Pichat, P.; Guillard, C.; Albini, A.; 1997. Probing the TiO2 photocatalytic mechanisms in water purification by use of quinoline, photofenton generated OH* radicals and superoxide dismutase, https://doi.org/10.1021/acs.jpcc.5b08630.

[6] Fujishima, A.; Rao, T. N.; Tryk, D. A.; 2000. Titanium dioxide photocatalysis, https://doi.org/10.4236/msce.2014.28004.

[7] Subramanian V, Wolf E, Kamat P: Semiconductor–metal composite nanostructures, to what extent do metal nanoparticles improve the photocatalytic activity of TiO2 films? J Phys Chem B 2001, 105:11439–11446.

[8] He C, Yu Y, Hu X, Hu A: Influence of silver doping on the photocatalytic activity of titania films. Appl Surf Sci 2002, 200:239–247.

[9] Alem A, Sarpoolaky H: The effect of silver doping on photocatalytic properties of titania multilayer membranes. Solid State Sci 2010, 12:1469–1472.

[10] Sobana N, Selvam K, Swaminathan M: Optimization of photocatalytic degradation conditions of direct Red 23 using nano-Ag doped TiO2. Sep Purif Technic 2008, 62:648–653.

[11] Sathishkumar P, Anandan S, Maruthamuthu P: Synthesis of Fe3+ doped TiO2 photocatalysts for the visible assisted degradation of an azo dye. Colloid. Surfaces A: Physicochem Eng Aspects 2011, 375:231–236.

[12] Pal B, Sharon M, Nogami N: Preparation and characterization of TiO2/ Fe2O3 binary mixed oxides and its photocatalytic properties. Mater Chem Phys 1999, 59:254–261.

[13] Liu H, Shon HK, Sun X, Vigneswaran S: Preparation and characterization of visible light responsive Fe2O3–TiO2 composites. Appl Surf Sci 2011, 257:5813–5819.

[14] Tong T, Zhang J, Tian B, Chen F, He D: Preparation of Fe3+-doped TiO2 catalysts by controlled hydrolysis of titanium alkoxide and study on their photocatalytic activity for methyl Orange. degradation J Hazard Mater 2008, 155:572–579.

[15] Litter MI: Heterogeneous photocatalysis transition metal ions in photocatalytic systems. J Appl Catal A: Environ 1999, 23:89–114.

[16] Wilke K, Breuer HD: The influence of transition metal doping on the physical and photocatalytic properties of titania. J Photochem Photobiol A: Chem 1999, 121:49–53.

[17] Wong RSK, Feng J, Hu X, Yue PL: Discoloration and mineralization of nonbiodegradable azo dye Orange II by copper-doped TiO2 nanocatalysts. J Environ Sci Health A 2004, 39:2583–2595.

[18] Devi LG, Kumar SG, Murthy BN, Kottam N: Influence of Mn2+ and Mo6+ dopants on the phase transformations of TiO2 lattice and its photo catalytic activity under solar illumination. Catal Commun 2009, 10:794–798.

[19] Devi LG, Kottam N, Murthy BN, Kumar SG: Enhanced photocatalytic activity of transition metal Mn2+, Ni2+ and Zn2+ doped polycrystalline titania for the degradation of Aniline Blue under UV/solar light. J Mo Catal A: Chem 2010, 328:44–52.

[20] Devi LG, Murthy BN, Kumar SG: Photocatalytic activity of TiO2 doped with Zn2+ and V5+ transition metal ions: Influence of crystallite size and dopant electronic configuration on photocatalytic activity. Mater Sci Eng B 2010, 166:1–6.

[21] Tian B, Li C, Gu F, Jiang H, Hu Y, Zhang J: Flame sprayed V-doped TiO2 nanoparticles with enhanced photocatalytic activity under visible light irradiation. J Chem Eng 2009, 151:220–227.

[22] Li H, Zhao G, Chen Z, Han G, Song B: Low temperature synthesis of visible lightdriven vanadium doped titania photocatalyst. J Colloid Interface Sci 2010, 344:247–250.

[23] Xu J, Ao Y, Chen M, Fu D, Yuan C: Photocatalytic activity of vanadiumdoped titania-activated carbon composite film under visible light. Thin Solid Films 2010, 518:4170–4174.

[24] Wu JCS, Chen CH: A visible-light response vanadium-doped titania nanocatalyst by sol–gel method. J Photochem Photobiol A: Chem 2004, 163:509–515.

[25] Sajjad AKL, Shamaila, Tian B, Chen F: One step activation of WOx/TiO2 nanocomposites with enhanced photocatalytic activity. Appl Catal B: Environ 2009, 91:397–405.

[26] Saepurahman, Abdullah MA, Chong FK: Preparation and characterization of tungsten-loaded titanium dioxide photocatalyst for enhanced dye degradation. J Hazard Mater 2010, 176:451–458.

[27] Hathway T, Rockafellow EM, Oh YC, Jenks WS: Photocatalytic degradation using tungsten-modified TiO2 and visible light: kinetic and mechanistic effects using multiple catalyst doping strategies. J Photochem and Photobiol A: Chem 2009, 207:197–203.

[28] Gandhe AR, Fernandes JB: A simple method to synthesize N-doped rutile tiania with enhanced photocatalytic activity in sunlight. J Solid State Chem 2005, 178:2953–2957.

[29] Sathish M, Viswanathan B, Viswanath RP, Gopinath CS: Synthesis, characterization, electronic structure, and photocatalytic activity of nitrogen-doped TiO2 nanocatalyst. Chem Mater 2005, 17:6349–6353.

[30] Wang YQ, Yu XJ, Sun DZ: Synthesis, characterization, and photocatalytic activity of TiO2–xNx nanocatalyst. J Hazard Mater 2007, 144:328–333.

[31] Li H, Wang D, Fan H, Wang P, Jiang T, Xie T: Synthesis of highly efficient C-doped TiO2 photocatalyst and its photo-generated charge-transfer properties. J Colloid Interface Sci 2011, 354:175–180.

[32] M.V. Dozzi, C. D'Andrea, B. Ohtani, G. Valentini, E. Selli, Fluorine- dope TiO2 materials: photocatalytic activityvs. time-resolved photolu- minescence, J. Phys. Chem. C 117 (2013) 25586–25595.

[33] L. Spanhel, H. Weller, A. Herglein, Photochemistry of semiconductor colloids. 22. Electron ejection from illuminated cadmium sulfide into attached titanium and zinc oxide particles, J. Am. Chem. Soc. 109 (1987) 6632–6635.

[34] K.R. Gopidas, M. Bohorquez, P.V. Kamat, Photophysical and photo- chemical aspects of coupled semiconductors: charge-transfer processes in colloidal cadmium sulfide-titania and cadmium sulfide-silver(I) iodide systems, J. Phys. Chem. 94 (1990) 6435–6440.

[35] R.J. Dillon, J. B. Joo, F. Zaera, Y. Yin, C. J. Bardeen, Correlating the exicited state relaxation dy namics as measured by photoluminescence and transient absorption with the photocatalytic activity of Au@TiO2 core-shell nanostructures, Phys. Chem. Chem. Phys. 15(2013)1488–1496.

[36] W. Lee, H.S. Shen, K. Dwight, A. Wold, Effect of silver on the photocatalytic activity of TiO2, J. Solid State Chem. 106 (1993) 288–294.

[37] M.C. Wang, H.J. Lin, T.S. Yang, Characteristics and optical properties of iron ion (Fe3þ)-doped titanium oxide films prepared by a sol–gel spin coating, J. Alloys Compd. 473 (2009) 394–400.

[38] F. Garcia, J.P. Holgado, L. Contreras, T. Girardeau, A.R. González-Elipe, Optical and crystallisation behaviour of TiO2 and V/TiO2 thin films prepared by plasma and ion beam assisted methods, Thin Solid Films 429 (2003) 84–90.

[39] . Zhu, W. Zheng, B. He, J. Zhang, M. Anpo, Characterization of Fe– TiO2 photocatalysts synthesized by hydrothermal method and their photocatalytic reactivity for photodegradation of XRG dye diluted in water, J. Mo. Catal. A: Chem. 216 (2004) 35–43.

[40] M. Zhou, J. Yu, B. Cheng, H. Yu, Preparation and photocatalytic activity of Fe-doped mesoporous titanium dioxide nanocrystalline photocatalysts, Mater. Chem. Phys. 93 (2005) 159–163.

[41] H. Tang, D. Zhang, G. Tang, X. Ji, W. Li, C. Li, X. Yang, Hydrothermal synthesis and visible-light photocatalytic activity of α-Fe2O3/TiO2 composite hollow microspheres, Ceram. Int. 39 (2013) 8633–8640.

[42] V.A. Ganesh, A.S. Nair, H.K. Raut, T.M. Walsh, S.Ramakrishna, Photocatalytic superhydrophilic TiO2 coating on glass by electrospinning, RSC Adv. 2 (2012) 2067–2072.

[43] T. Ohnu, F. Tanigawa, K. Fujihara, S. Izumi, M. Matsumura, Photocatalytic oxidation of water by visible light using ruthenium-doped titanium dioxide powder, J. Photochem. Photobiol. A: Chem. 127 (1999)107–110.

[44] R.S. Sonawane, B.B. Kale, M.K. Dongare, Preparation and photo- catalytic activity of Fe-TiO2 thin films prepared by sol-gel coating, Mater. Chem. Phys. 85 (2004) 52–57.

[45] L. Huang, T. Liu, H.Zheng, W.Guo, W. Zeng, Hydrothermal synthesis of different TiO2 nanostructures: structure, growth and gas sensor properties, J. Mater. Sci.: Mater. Electron. 23 (2012) 2024–2029.

[46] G.N. Schrauzer, T.D. Guth, Photocatalytic reactions. 1. Photolysis of water and photoreduction of nitrogen on titanium dioxide, J. Am. Chem. Soc. 99 (1977) 7189–7193.

[47] S.B. Amor, G. Baud, J.P. Besse, J. Jacquet, Structural and optical properties of sputtered Titania films, Mater. Sci. Eng. B47 (1997) 110–118.

[48] C.R. Ottermann, K. Bange, Correlation between the density of TiO2 films and thei rproperties, Thin Solid Films 286 (1996) 32–34

[49] A. Rampaul, I.P. Parkin, S.A. O' Neill, J. DeSouza, A. Mills, N. Elliott, Titania and tungsten doped titania thin films on glass; active photo- catalysts, Polyhedron 22 (2003) 35–44.

[50] C.J. Brinker, G.W. Scherer, Sol–Gel Science, Academic Press, San Diego, CA, 1990.

[51] H. Bensouyad, D. Adnane, H. Dehdouh,B. Toubal, M. Brahimi, H. Sedrati R. Bensaha, J Sol-Gel Sci Technol DOI 10.1007/s10971-011-2525-5.

[52] R. Mechiakh, R. Bensaha, C.R. Phys. 7 (2006) 464.

[53] H. Bensouyad , H. Sedrati , H. Dehdouh , M. Brahimi , F. Abbas , H. Akkari , R. Bensaha, Thin Solid Films 519 (2010) 96.

[54] R. Mechiakh, R. Bensaha, M. J. Condensed. Mater. 7 (2006) 54.

[55] D. Komaraiah, E. Radha, N. Kalarikkal, J. Sivakumar, M.V. Ramana Reddy,R. Sayanna, Structural, optical and photoluminescence studies of sol-gel synthesized pureand iron doped TiO2photocatalysts, Ceram. Int. (2019),https://doi.org/10.1016/j.ceramint.2019.03.170.

[56] D. Komaraiah, E. Radha, J. James, N. Kalarikkal, J. Sivakumar, M.V. RamanaReddy, R. Sayanna, EfEffect of particle size and dopant concentration on the Raman and thephotoluminescence spectra of TiO2:Eu+3nanophosphorthinfilms, J.Lumin. 211 (2019) 320–333.

[57] N.T. Mc Devitt and al., Spectrochimica, Act, 20, 799, (1964).

[58] K. CHHOR, J.F. BOCQUET and C. POMMIER, Matr. Chem. Phy, 32,(1992) ,249
[59] LARBOT, I.LAAZIZ, J. MARIGNAN and J.F. QUINSON,Non_crystall. Solids, 157, 148, (1992).
[60] R. Ramesh, K. Ashok, G. M. Bhalero, S. Ponnusamy, C. Muthamizhchelvan. Cryst. Res
[61] Technol. 45(2010) 965-968.
[62] S. A. Alim, T. S. Rao, I. M. Raju, M. R. Kumar, K.V. D. Lakshmi, Journal of SaudiChemical Society, 23 (1) (2019) 92.